Influence of compaction on the soil shrinkage and swelling curves

David Encalada[1*]*, Abdallah* Najdi[1,2]*, Joao* Mendes[3]*, Pere* Prat[1], and *Alberto* Ledesma[1]

[1] Dept. of Civil and Environmental Engineering, UPC - Barcelona Tech, Jordi Girona, 1-3, D2, 08034 Barcelona, Spain
[2] Dept of Mechanical and Construction Engineering, Northumbria University, NE1 8ST, Newcastle upon Tyne, UK
[3] Dept. of Civil Engineering, Newcastle University, Newcastle, UK

Abstract. The behaviour of soils undergoing deformation due to changes in water content can be described using Soil Shrinkage Curves (SSCs). The SSCs are normally influenced by several factors as the soil's fabric, different compaction levels, residual void ratio, and the shrinkage limit. In this study, shrinkage curves at different compaction levels were obtained using both wax coating and image analysis as volumetric quantification methods. Both techniques returned consistent results. To fit the obtained experimental data, a single equation is proposed with fitting parameters pertaining to the physical characteristics of the soil samples used. The use of Mercury Intrusion Porosimetry (MIP) is also incorporated to further analyse the structure of the soils being studied. The effect of the drying path on the structure was more apparent in the size range of 100-2000 nm. The effects of compaction on soil structure and shrinkage behaviour were also discussed in the study. The presented work provides valuable insights on the effect of different compaction levels on the soil shrinkage behaviour.

1 Introduction

Shallow layers of soil are at constant interaction with the overlaying atmosphere, leading to continuous moisture transfer in between the two mediums, which directly affects the soil's hydro-mechanical behaviour. One significant effect of the soil-atmosphere interaction is the shrinkage and swelling experienced by the topsoil layers due to the changes in moisture content that occur. The shrinkage and swelling behaviour can cause cracking, which leads to the destabilisation of the soil structure, and consequently leading to an increase in the risk of landslides, and to a decrease in the capacity of soil to retain water [1, 2].

Soils exposed to drying due to porewater evaporation are expected to undergo changes in the pore structure and may experience volumetric changes. The relationship between changes in porewater content and the void ratio of drying soils is often depicted in a Soil Shrinkage Curve (SSC). SSCs have long been used to study the performance of drying soils, and the volumetric changes due to imposed drying paths can be divided into four stages: structural, proportional, residual, and zero-shrinkage [1, 3]. However, remoulded soil specimens (i.e., compacted or slurry conditions) typically exhibit the last three stages only.

Soil shrinkage curves normally cannot be considered unique nor an intrinsic property of the material being studied. In fact, varying SSCs can be obtained for the same material depending on the initial placement conditions. There are numerous established formulas in the literature that describe the SSC and express the void ratio as a function of varying water content [4, 5]. However, the fitting parameters are not always directly related to the physical phenomena being studied, and it may be necessary to use multiple equations to involve the physical meaning [6].

It is well established that compaction has a significant influence on soil structure [7]. Soil compacted at low water content tends to have a double porosity structure, while soil compacted at optimum water content and in the wet range typically has a monomodal pore size distribution (PSD). To better understand the changes in soil structure during the desiccation process, it is necessary to compare the PSD at various water content stages.

The objective of this study is to propose a new single equation capable of fitting the shrinkage behaviour. The fitting parameters are associated with intrinsic characteristics of the phenomenon, which results in a more comprehensive understanding of the SSC. Two volumetric measurement methods were employed under different conditions: wax coating (WC) with paraffin and digital image analysis (DIA). The former method estimates the volume through water displacement, while the latter estimates the volume from the change in area and height of the samples [8, 9]. Additionally, the influence of compaction on soil fabric and structure is explored through the analysis of the PSD.

2 Material and methods

---

* Corresponding author: david.encalada@upc.edu

2.1 Material

The soil tested in this investigation was a silty clay from Agròpolis site. This soil has been characterized in previous investigations, and its most relevant proprieties are summarized in Table 1.

Before the sample preparation, the soil was air dried and crushed, and the coarse particles were removed using a 2mm sieve.

Table 1. Index properties of the Agròpolis silty clay. [10]

Property	Value
Sand content ($\leq$ 2mm)	48.3%
Silt content ($\leq$ 63μm)	42.1%
Clay content ($\leq$ 2μm)	9.6%
Unit weight of solid particles	27 kN/m^3
Liquid limit (w_L)	29%
Plastic limit (w_P)	17%
Unified soil classification system	CL

2.2 Density

Several batches of soil with different water content were prepared by carefully mixing the soil with water and sealing the mixtures in plastic bags to allow them to homogenise for at least 48 hours.

Cylindrical soil specimens with a diameter of 50 mm and a height of 20 mm were prepared at different initial conditions in terms of water content and dry density, with the goal of replicating the energy compaction of the Standard and Modified Proctor compaction tests (593.7 kJ/m^3 and 2693.3 kJ/m^3, respectively). Additionally, slurry samples were prepared with the same initial geometry. The experimental program is summarized in Table 2.

After compaction, the samples were set to rest for an additional period for moisture homogenisation. Then, the samples were dried in a laboratory with open air conditions (T 20°C and RH 50%). The evolution volumetric deformation was monitored using two techniques: volume displacement with paraffin coating and digital image analysis.

2.2.1 Wax coating

Samples were dried to reach different target levels of water content. To explore the hysteresis of volumetric deformation, some samples were dried to reach equilibrium with the environment, and then carefully wetted using water droplets at the top surface, avoiding any damage to the sample integrity. The sample was allowed to rest for a minimum of 2h between each wetting step. It was assumed that when free water starts to appear at the bottom of the sample, it indicates that the sample has reached its limit of water storage. Finally, some sample were exposed to a second drying cycle.

Table 2. Experimental program.

Batch	State	w_0 (g/g)	e_0 (-)
12S	Standard compaction	12	0.53
15S		15	0.52
17S		17	0.50
21S		21	0.61
12M	Modified compaction	12	0.39
15M		15	0.46
32SL	Slurry	32	0.89
36SL		32	1.00
40SL		40	1.10

2.2.2 Image analysis

A single soil specimen was placed at a time on the scale, to record the weight at a 10 min interval. Digital images were taken at a 1 h interval inside a white lightbox to maintain a consistent light intensity. Two digital cameras were used to track the vertical and horizontal deformation, simultaneously. A non-shiny plastic plate, of a distinctive colour from that of the soil, was placed under the specimen, to obtain greater contrast in the image between the specimen and the background. The cameras captured images with a minimum resolution of 46 pixels/mm in both vertical and horizontal displacements.

The first camera was positioned at 30 cm above the soil sample. The change in the area is segmented by thresholding. The out-of-plane motion affects the image magnification, and is proportional to $\Delta z/z$; where Δz is the out-of-plane displacement and z is the distance from the object to the camera [11]. However, the out-of-plane motion effect can be safely neglected due to the distance from the object to the camera being sufficiently large with respect to the expected values of Δz.

2.3 Pore size distribution

The pore structure of soil was examined using mercury intrusion porosimeter (MIP). The equipment used was a Micromeritics Auto Pore IV 9500. Two small samples, each about 10 mm in diameter and height, were taken from different batches (12S, 17S, 21S, 12M and 15M; Table 2). One sample was dried at room conditions, while the other was handled using the lyophilization technique to extract the water without causing any shrinkage and altering its initial condition structure [12].

3 Shrinkage Curve equation

Soil shrinkage curves can be normally divided into four stages: structural, proportional, residual, and zero-

shrinkage. The structural shrinkage stage is of that of wormholes and macropores. SSCs starting at the structural shrinkage stage can be referred to as having an S-shaped curve. However, in the case of remoulded specimens with no macropores, the SSCs are expected to initiate at the proportional shrinkage stage and can be referred to as having a J-shaped curve.
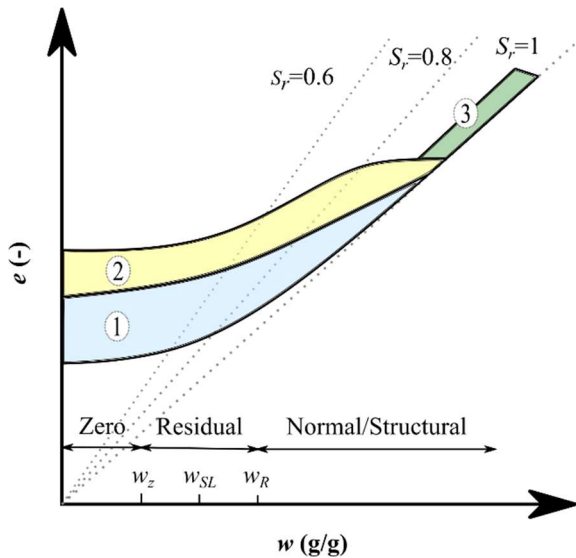

Fig. 1. Region of possible family of shrinkage/swelling curves.

Fig. 1 shows a generalised set of SSCs, where 3 different zones can be identified. Zones 1 and 2 are for soils in solid state. Zone 1 is where SSCs are J-shaped, i.e., absence of structural shrinkage. Zone 2 is where SSCs are S-shaped. Zone 3 is where the material starts in a liquid state and transitions to a solid state with a characteristic J-shaped curve. The J-shaped curves has two stage limits: w_R and w_Z. In a drying state, w_R represents the end of normal shrinkage stage, and is often referred to as the air-entry value. w_z refers to the zero-shrinkage stage, the water content beyond which no significant deformation is expected to occur due to drying. The shrinkage limit (w_{SL}) is typically located between these two values, considering that some studies [13] may define w_{SL} as w_Z. The value of w_{SL} can be obtained graphically by the intersection of the lines of zero and normal shrinkage stages [4, 14].

The proposed model equation can be given in the form:

$$e = \frac{a}{c}\ln\left(\frac{\exp(bc)+\exp(cw)}{\exp(bc)+1}\right) + d \qquad (1)$$

where w is the gravimetric water content, d is the void ratio at zero-shrinkage (e_{min}) and a, b and c are fitting parameters that control the shape of the curve. The fitting parameters can be directly related to the soil characteristics and parameters. For instance, the fitting parameter a is the slope of the curve within the normal shrinkage stage. Parameter b is equal to the shrinkage limit (w_{SL}) and c controls the duration of the residual stage. The value of c is equal to:

$$c = \frac{4}{w_R - w_Z} \qquad (2)$$

In this model the value of w_{SL} is assumed as mid distance between w_R and w_Z.

$$b = w_{SL} = \frac{w_R + w_Z}{2} \qquad (3)$$

After the fitting it is possible to obtain the values of w_R, w_{SL} and w_z or the fitting parameter could be obtained from the limits of each stage.

The proposed model is then compared to the most widely used ones encountered in the literature. The comparison is carried by presenting the number of parameters and the shape of the curve. Cornelis et al. [5] present an equation that has the advantage of modelling both normal and structural shrinkage but has the least number of physical parameters. Fredlund et al. [4] model has one more physical parameter in common with ours - the normal shrinkage slope (a). While each model has its benefits, such as simplicity or shape, our model stands out for having all parameters with a physical meaning.

Table 3. Experimental program.

Equation	Parameters		Curve
	Total	Physical	
This study	4	4	J-shaped
Fredlund et al. [4]	3	2	J-shaped
Cornelis et al. [5]	4	1	J-shaped or S-shaped

The behaviour of parameters b and c on the equation are illustrated in Fig. 2. All the curves were generated using a fixed value of $a = 2.7$ and $d = 0.40$. A change in parameter b from 0.15 to 0.20 resulted in a displacement of the w_{SL} point. Additionally, as parameter c decreased from 100 to 40, we observed an increase in the difference between w_R and w_Z, indicating an increase in the range of residual stage.
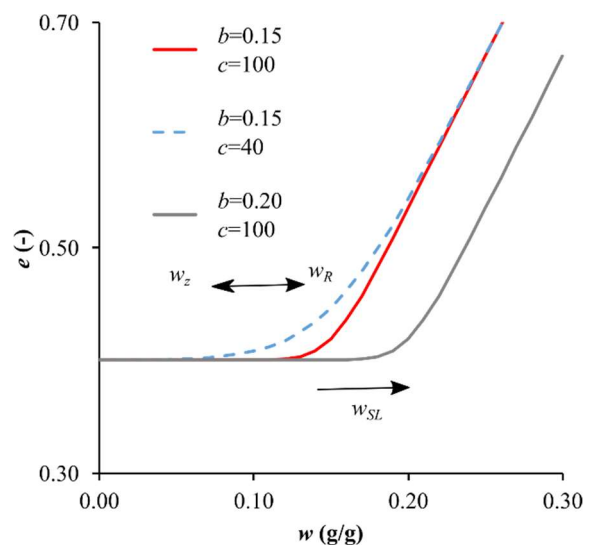

Fig. 2. Effects of parameters b and c.

4 Results and discussion

4.1 Shrinkage and swelling curves

Fig. 3 presents the results with the two different volumetric measurement methods for compacted specimens following first drying (D), wetting (W) and second drying (D2) paths. The results in the figure are partially plotted to avoid overwhelming the graph and to distinguish the drying and wetting paths. However, the complete data will be presented later at section 4.2. All the obtained SSCs were J-shaped with significant hysteresis between the drying and wetting paths. The main differences in the curves can be attributed to the minimum void ratio, the slope during normal shrinkage, and the value of w_{SL}. For example, the 12S and 12M batches have the same initial water content but different compaction levels.
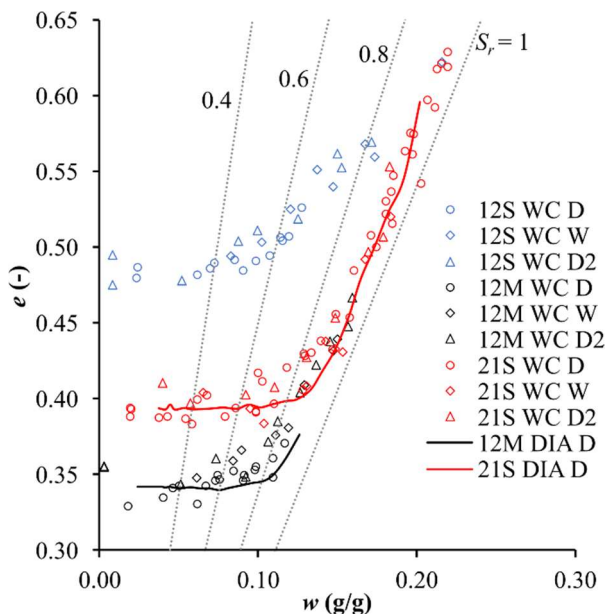

Fig. 3. Compacted specimens

In the wet path, the specimens reach water content around 0.21 without any collapse observed by crumbling or cracking. The overall pattern of the volumetric measurement results was similar for both the methods used. However, the data obtained by WC exhibits greater scatter opposed to the more consistent DIA results.

The experimental data of the slurry samples are presented in Fig. 4. The initial volumetric measurements for the drying path were estimated from the volume of the container. At a large scale, a unique trend J-shaped curve with no significant hysteresis is observed. Nonetheless, it may be considerably larger if we observe that the minimum void ratio varies around 0.40 and 0.50. Entrapped air was normally encountered in slurry specimens, which may lead to more dispersed values in the experimental results.

4.2 Model fitting

The obtained model fitting parameters and the coefficient of determination (R^2) are summarized in

Table 4. The values of R^2 were found to be close to 1.0, with the exception of batch 15S, where the value was 0.78 due to the high scatter present in the experimental data.
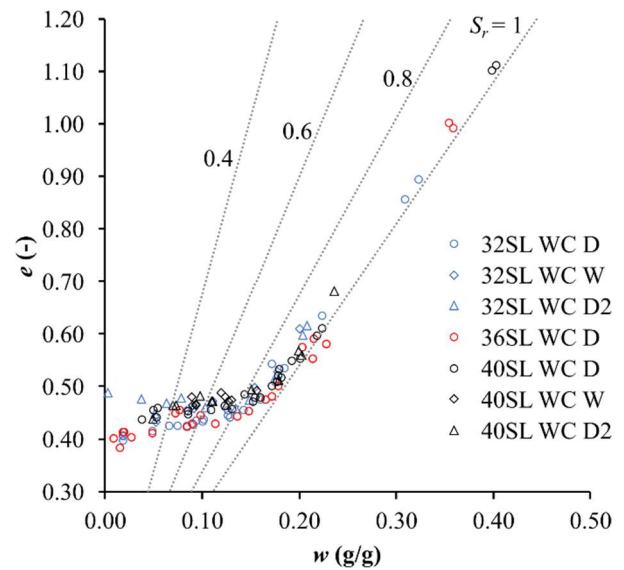

Fig. 4. Slurry specimens

Batch 12S was found to have a relatively low value of a equal to 1.11, while other batches had steeper slopes. Additionally, e_{min} varies from 0.34 to 0.48 and depends on the compaction level, as well as the stress history. It is noteworthy that slurry specimens have lower values of e_{min} compared to compacted batches 12S and 15S. The value of w_{SL} ranges from 0.09 to 0.17, with less compacted soils tending to have a value closer to zero. As with respect to parameter c, compacted soils were found to have higher values ranging from 60 to 100, while in slurries the values were close to 40. This suggests that the residual stage spans larger along the water content axis in compacted soils than in slurries.

The characteristic limits of the shrinkage stages (w_Z and w_R) can be then obtained from the fitting parameters using the relations explained in equations (2) and (3). The obtained values are presented in table 4.

The fitting results of the proposed equation with the presented fitting parameters against the experimental data are presented in Fig. 5.

4.3 Pore size distribution

The PSD for both specimens compacted with standard and modified proctor efforts are shown in Fig. 6 and Fig. 7, respectively. Sample 12S shows a clear bimodal shape, while the remaining samples exhibit a monomodal shape. The peak particle size is consistent across all samples, with a range of 150-500 nm. The lower range, below 100 nm, remains unchanged. A consistent observation in all samples is the reduction of peak size from the as compacted conditions after the drying process, with no notable alteration of the dominant pore size. This trend aligns with previous studies reported in the literature [15]. The higher changes in PSD happens on pores with diameter between 100 nm and 2000 nm.

Table 4. SSC fitting parameters.

Batch	*a*	*b (w_SL)*	*c*	*d (e_min)*	R^2	*w_Z*	*w_R*
12S	1.11	0.09	59.9	0.481	0.95	0.023	0.157
15S	1.07	0.10	100.0	0.460	0.78	0.060	0.140
17S	3.30	0.14	57.4	0.374	0.92	0.068	0.207
21S	2.75	0.13	72.6	0.393	0.99	0.078	0.188
12M	2.43	0.11	78.0	0.343	0.93	0.059	0.161
15M	2.79	0.13	75.1	0.367	0.89	0.072	0.179
32SL	2.50	0.13	40.9	0.416	0.96	0.037	0.232
36SL	2.87	0.16	40.9	0.402	0.97	0.057	0.253
40SL	2.81	0.17	41.0	0.455	0.99	0.072	0.267

Fig. 5. Curve fitting.

Fig. 6. Evolution of PSD with drying for low compaction energy specimens.
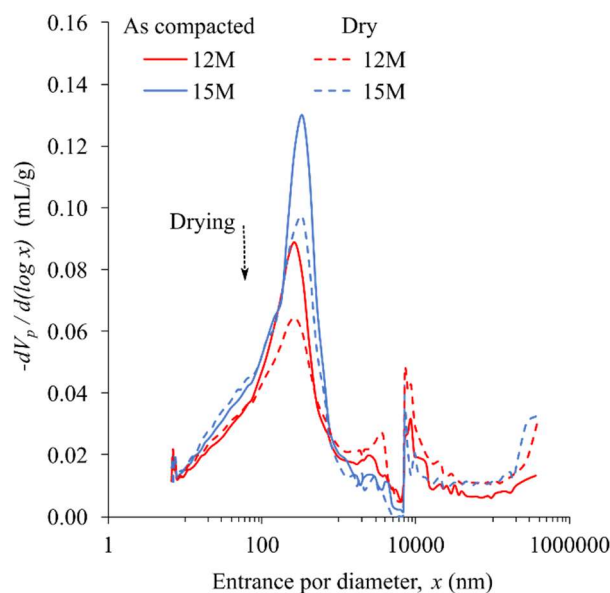
Fig. 7. Evolution of PSD with drying for high compaction energy specimens.
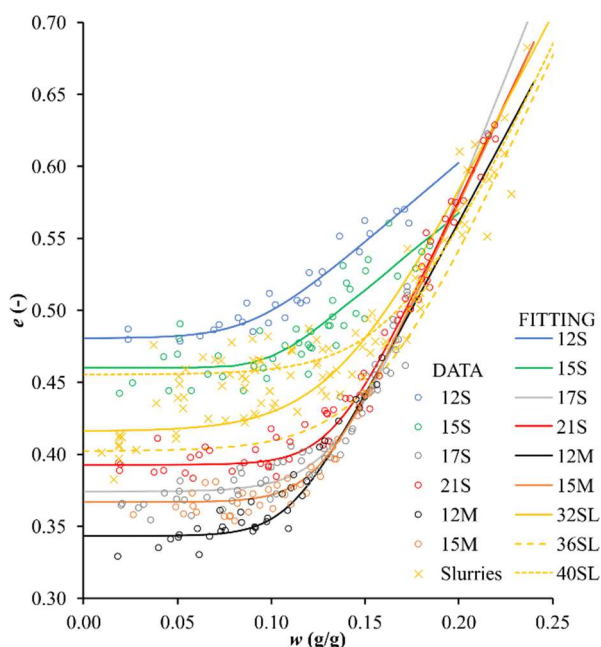
The distinction between micro and macro porosity is not clearly defined in the literature. One commonly used method is to use the value obtained from mercury intrusion and extrusion curves, which in this study was found to be in the range of 180-240 nm. However, it is important to note that this method has been criticized for being inadequate, as the value is often located close to the peak [16] and may not accurately reflect the size of the pores. An alternative approach is to use the lowest point of the valley between the two peaks of a bimodal PSD of samples, which is around 2000 nm when using the PSD of batch 12S as a reference. This criterion suggests that significant changes in microporosity occur during the drying path, which can help explain the variations in the SSC of batches 12S and 15S.
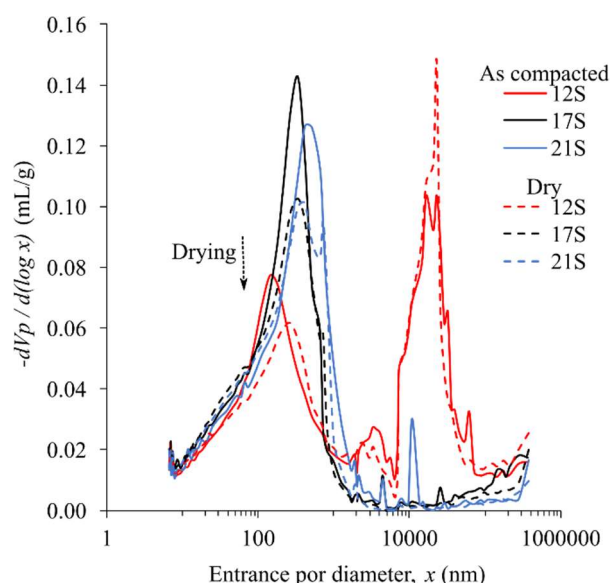
5 Conclusion

Multiple shrinkage characteristic curves (SSCs) were obtained at different compaction levels using two different volumetric measurement methods. The limitations of the wax coating (WC) method include the ability to only obtain a single point of the SSC per specimen and the need for multiple samples to fully describe the SSC, leading to scattered results. Non-contact methods such as image analysis may be a more suitable alternative for highly wet samples, which are prone to destruction during manipulation. The study also found that there was no significant hysteresis observed in the curves during the drying and wetting process. The experimental results indicate that soil compacted at low initial water content tends to have a flatter slope during the residual shrinkage stage, and a higher residual void ratio, suggesting that deformation occurs mainly in micropores. The proposed equation was found to be effective in fitting J-shaped curves and connecting the fitting parameters to more descriptive values of the phenomena.

References

1. J. J. B. Bronswijk, Soil Sci, 145 (1991)

2. Q. F. Gao, L. Zeng, Z. N. Shi, Comput Geotech. Elsevier Ltd, **140**, 104436 (2021)

3. W. B. Haines, J Agric Sci. Cambridge University Press, **13**, 296–310 (1923)

4. M. D. Fredlund, G. W. Wilson, D. G. Fredlund 3rd Int. Conf. Unsaturated Soils, UNSAT 2002, 145–9 (2002)

5. W. M. Cornelis, J. Corluy, H. Medina, J. Díaz, R. Hartmann, M. Van Meirvenne, et al., Geoderma, **137**, 179–91 (2006)

6. P. Chen, N. Lu, J Geotech Geoenvironmental Eng, **144**, 1–10 (2018)

7. A. Tarantino, E. De Col, Geotechnique, **58**, 199–213 (2008).

8. A. J. Puppala, B. Katha, L. R. Hoyos, Geotech Test J, **27**, 547–56 (2004)

9. A. C. Amenuvor, G. Li, J. Wu, Y. Hou, W. Chen, Geoderma, **363**, 1–7 (2020).

10. J. A. Cordero, A. Cuadrado, P. Prat, A. Ledesma 3rd Eur Conf Unsaturated Soils, E-UNSAT. Paris: EDP Science, 12005, 1-6 (2016)

11. M. A. Sutton, J.H. Yan, V. Tiwari, H.W. Schreier, J. J. Orteu, Opt Lasers Eng, **46**, 746–57 (2008)

12. E. Romero, G. Della Vecchia, C. Jommi, Geotechnique, **61**, 313–28 (2011)

13. E. C. Leong, M. Wijaya, Geoderma, **237**; 78–87 (2015)

14. P. R. N. Hobbs, L. D. Jones, M. P. Kirkham, D. A. Gunn, D. C. Entwisle, Q J Eng Geol Hydrogeol, **52**, 220–9 (2019)

15. X. Liu, O. Buzzi, S. Yuan, J. Mendes, S. Fityus, Can Geotech J, **53**, 854–70 (2016)

16. S. Yuan, X. Liu, E. Romero, P. Delage, O. Buzzi, Geotech Lett, **10**, 454–60 (2020)